Elastic Proton-Deuteron Scattering at 450 Mev*

A. V. CREWE,† B. LEDLEY, E. LILLETHUN, S. MARCOWITZ, AND L. G. PONDROM‡
The Enrico Fermi Institute for Nuclear Studies, The University of Chicago, Chicago, Illinois

(Received January 9, 1959)

The elastic scattering cross section for 450-Mev protons by deuterons has been measured for proton center-of-mass scattering angles from 16.45° to 127°. The scattered protons (or recoil deuterons) were analyzed by a magnet and detected by a scintillation counter telescope. The cross sections have been normalized by using published *p-p* cross sections. The sticking factor has been calculated for two deuteron potentials using the impulse approximation. This analysis indicates that there may be destructive interference between the *n-p* and *p-p* scattering in the deuteron at this energy.

INTRODUCTION

SEVERAL experiments have been performed on elastic proton-deuteron scattering at high energies, notably those of Chamberlain and Clark at 340 Mev[1] and Schamberger at 240 Mev.[2] The main experimental difficulty in going to higher energies than this is the problem of distinguishing between purely elastic scattering and slightly inelastic scattering. In this experiment, the separation was achieved by means of a magnetic spectrometer.[3]

The interest in this experiment lies in the attempt to correlate the experimental results with the known data on nucleon-nucleon scattering. The most detailed analysis of proton-deuteron scattering so far has been carried out by Chamberlain and Stern.[4] We use their approach to interpret our results.

Using the method of the impulse approximation,[5] the differential scattering cross section for elastic proton-deuteron scattering can be written[4]

$$\frac{d\sigma_{pd}}{d\Omega}(\theta)=\frac{16}{9}S(\theta)\left[\frac{d\sigma_{pp}}{d\Omega}(\theta',T_0')+\frac{d\sigma_{np}}{d\Omega}(\theta',T_0')\right]\Delta, \quad (1)$$

where S is the so-called "sticking factor";

$$S(\theta)=\int\psi_d{}^2\exp\left[i\left(\frac{\mathbf{k}\cdot\mathbf{r}}{2}\right)\right]d\mathbf{r}, \quad (2)$$

and ψ_d is the ground-state wave function of the deuteron. $\mathbf{k}$ is the momentum transfer in the elementary nucleon-nucleon collision. (For a detailed discussion of the co-ordinate system, see reference 5.)

The differential cross sections for *n-p* and *p-p* collisions which occur on the right-hand side of Eq. (1) are to be evaluated at angles θ' and energies T_0' defined in Eqs. (3) and (4). Δ is a factor which is equal to unity in the absence of interference between *p-p* and *n-p* scattering, is greater than unity for constructive interference, and is less than unity for destructive interference.

One possible approach in the interpretation of the experimental results is to demonstrate the validity of Eq. (1) insofar as this is possible without having a detailed knowledge of the factor Δ. Therefore, we compare the theoretical quantities $S(\theta)$, obtained from Eq. (2) using generally accepted expressions for ψ_d, with $S(\theta)\Delta$ computed from Eq. (1) using experimental information only.

EXPERIMENTAL EQUIPMENT

The external beam of the University of Chicago synchrocyclotron (C) (Fig. 1) is focused by two quadrupole strong-focusing magnets (SM), forming a beam

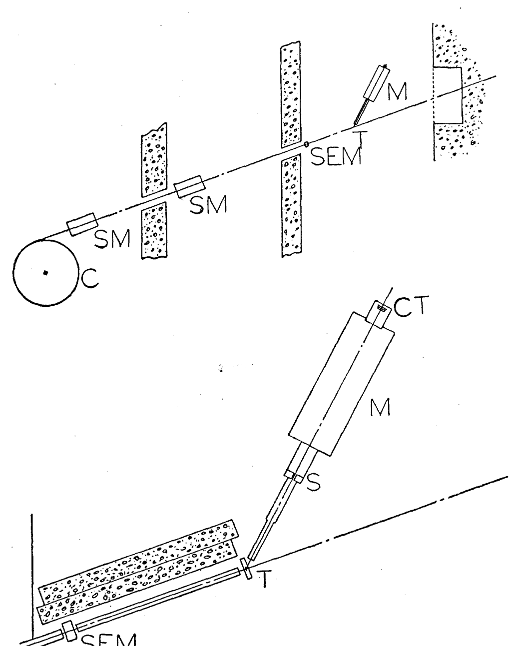

FIG. 1. Plan view of the experimental setup: Cyclotron, C; Strong Focus Magnets, SM; Secondary Emission Monitor, SEM; Target, T; Spectrometer Magnet, M; Aperture, S; and Counter Telescope, CT. Shaded sections represent concrete shielding.

* Research supported by a joint program of the Office of Naval Research and the U. S. Atomic Energy Commission.
† Also at Argonne National Laboratory, Lemont, Illinois.
‡ Now at Wright-Patterson Air Force Base, Dayton, Ohio.
1 D. D. Clark and O. Chamberlain, Phys. Rev. 102, 473 (1956).
2 R. D. Schamberger, Phys. Rev. 85, 424 (1952).
3 A. V. Crewe, Rev. Sci. Instr. 29, 880 (1958).
4 O. Chamberlain and M. O. Stern, Phys. Rev. 94, 666 (1954).
5 G. F. Chew, Phys. Rev. 74, 809 (1948).

spot about $\frac{3}{4}$ in. in diameter in the experimental area some 70 feet from the cyclotron. The proton beam travels in vacuum for the whole of this distance and has an intensity of about 2×10^{10} protons per second. The beam intensity is monitored by a secondary emission monitor[6] (*SEM*).

Two targets (*T*) were used; the first one was CD_2 wax, compression molded, of thickness 0.798 g/cm^2 $\pm1.7\%$, and the second one was of polymerized CD_2 of thickness 0.761 g/cm$^2\pm1.5\%$ similarly prepared. In each case matching carbon targets were used to subtract the effect of the carbon. The targets were mounted on a remotely controlled rotating target changer capable of holding twelve 2-in.×2-in. targets. Also mounted on the target changer were a matching pair of CH_2 and C targets which were used to measure the solid angle of acceptance of the magnet. The H_2 impurity in the CD_2 was stated to be 4% by the suppliers.

The spectrometer $(M)^3$ consists of a vertically deflecting magnet. The detecting counter telescope was mounted rigidly on the magnet, which can be rotated about the target. The magnet can approach within 7° of the forward direction without intercepting the primary beam of particles.

The magnet has a vacuum system which extends from the target to the counter telescope (*CT*). The entrance pipe to the magnet terminates in a thin Mylar window a few millimeters from the target, and the exit pipe has an aluminum window two inches in front of the first counter.

The entrance aperture (*S*) of the magnet consists of a rectangular opening 1 in.×3 in. in a 5-in. thick block of steel. This aperture is adjustable with the aid of spacer blocks. The beam of particles which emerges from the magnet is convergent in one direction and divergent in the other. Consequently, the defining counter must be in the shape of a long rectangle.[3] 6-in. long counters are adequate to detect all particles which emerge from the magnet. The width was chosen to be $\frac{1}{4}$ in. in order to achieve a counter resolution of about 0.5%. The actual counter telescope that was

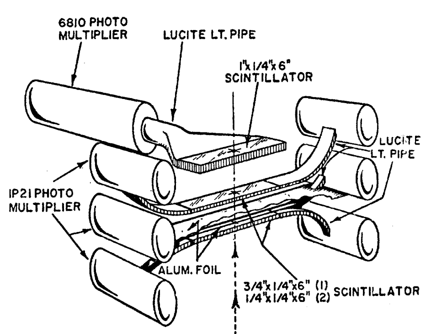

FIG. 2. Counter telescope. Particle beam of about 5 in. width enters from below.

[6] H. R. Fechter and G. W. Tautfest, Rev. Sci. Instr. **26**, 229 (1955).

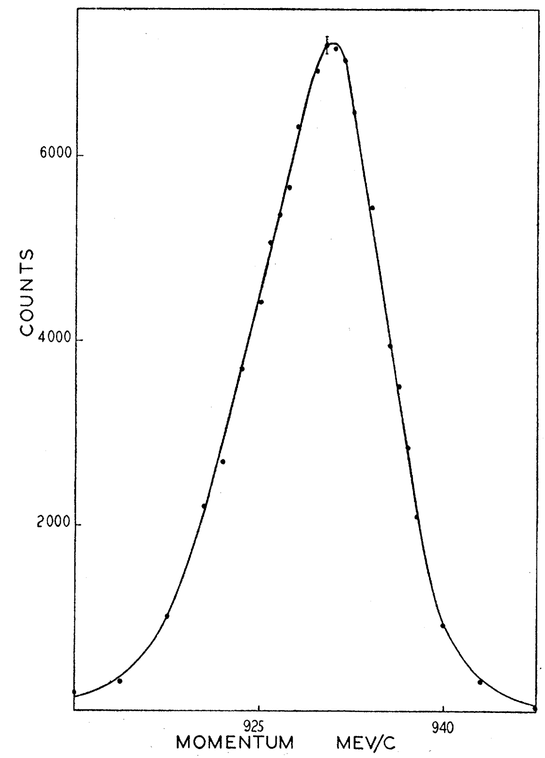

FIG. 3. A proton-proton peak used for calibration of the entrance aperture of the spectrometer magnet. Typical statistical error is shown at one point.

used is shown in Fig. 2. There were two identical defining counters mounted side by side. Each one was viewed from the ends by two 1P21 phototubes. These counters are designated 1A and 1B. Behind these counters was placed a third one, number 2, which was also viewed by two 1P21 phototubes. A fourth counter, number 3, was placed behind this and was viewed from the side by a 6810A phototube.

In each of the counters 1A, 1B, and 2, the pulses from the two 1P21 tubes were added. In this way, loss of pulse height due to loss of light was minimized. The voltages on the 1P21 tubes could be adjusted indedependently. 1A, 2, 3, and 1B, 2, 3 pulses were amplified and fed into separate fast coincidence circuits. The sizes and distances between the counters were chosen so that background counts were minimized.

The current flowing through the magnet was measured by means of a potentiometer connected across a shunt. The magnet was regulated with a dc amplifier system and the current could be held constant to 1 part in 10 000 over a period of many minutes. All values of the magnet current are given in millivolts, the conversion factor being 1 millivolt = 25 amp.

EXPERIMENTAL METHOD

The transparency of the entrance aperture of the magnet in the horizontal direction was checked by scanning a $\frac{1}{4}$-in.$\times\frac{1}{4}$-in. counter across the magnet face. This counter was placed in coincidence with the counter telescope at the focus. The transparency in the vertical direction was checked by reducing the vertical aperture with spacer blocks and observing the resultant reduction in the number of counts. It was found that an aperture of 1 in.$\times 2\frac{1}{2}$ in. could be used safely. It was felt that small angle scattering from the faces of the slit would be a problem, and this was checked by placing anticoincidence counters in such a position as to shield these faces from direct illumination from the target. The shape of a magnet curve taken with these counters in position was identical to that taken without the counters, except for a reduced area. In this way it was shown that slit-scattering effects were negligible.

The solid angle of acceptance of the magnet was determined by measuring the *p-p* differential cross section at two angles. A CH_2 and matching C target were placed alternately in position, and a magnet scan over the *p-p* peak was performed (Fig. 3). In this way, our calibration was made against the known *p-p* scattering cross section instead of the measured aperture. This eliminated the problem of allowing for the effect of the fringe magnetic field which distorts the orbits near the collimator.

The elastic proton-deuteron scattering cross sections were measured in the same way. However, in this case there was a choice of particle to be observed. Either the proton or the deuteron could be selected. It was an advantage wherever possible to use the deuteron because it gives a symmetric peak. The inelastic scattering of the proton produces an asymmetric peak and makes the measurement of the area of the elastic peak more difficult. However, there was only a small range of angles where the deuteron could easily be used. In the forward direction the momentum of the recoil deuteron is very high and the magnet could not be used. At large angles the momentum of the deuteron is low and energy loss in the target produced too wide a peak. These difficulties are illustrated by Fig. 4, where the momenta of the two particles are shown as a function of angle in the laboratory system and the limitations of the equipment are indicated.

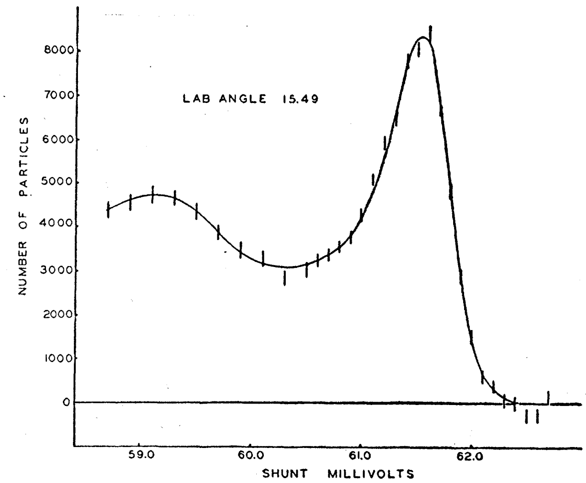

(a)

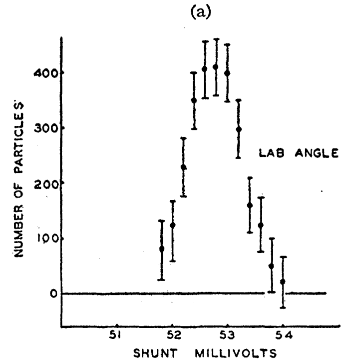

(b)

FIG. 5. (a) Peak showing protons scattered by deuterons *versus* magnet current. The asymmetry is due to inelastic scattering. (b) Deuteron peak from *p-d* elastic scattering. There are no inelastic events, so the peak is symmetric.

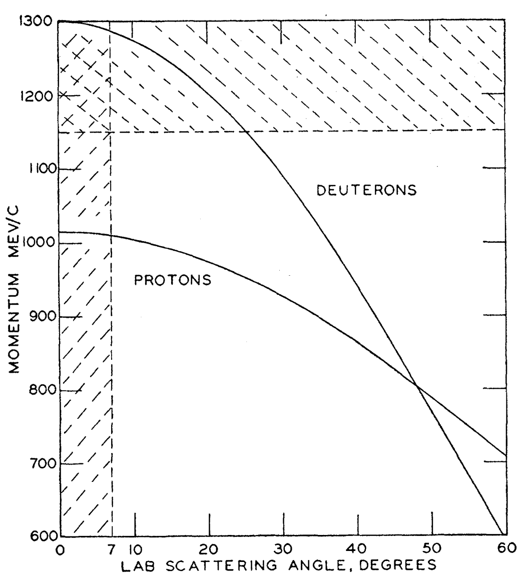

FIG. 4. Diagram showing momentum as a function of laboratory angle for protons and deuterons from *p-d* elastic scattering. The shaded parts indicate limitations of the equipment.

Figure 5 shows two magnet scans. Figure 5(a) is a proton peak and the inelastic component can be clearly seen. Figure 5(b) is a deuteron peak and, although there is no confusion due to inelastic events, the statistics are not very good. This was the poorest peak that was measured. It represents about 12 hours of running time.

In the case of the deuteron peaks, the area was calculated directly using the trapezoidal rule. For the proton peaks, the position of the center of the peak was estimated by symmetrizing the top portion of the curve. The area of the right-hand half of the peak was then calculated and multiplied by two. The error placed on the area was computed from statistical errors and the uncertainty in positioning the center of the peak.

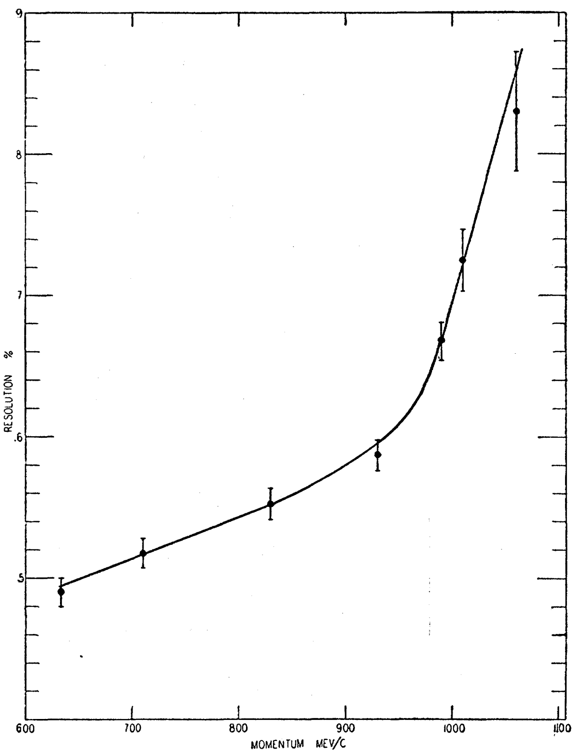

FIG. 6. Magnet resolution as a function of particle momentum. The numbers on the left-hand side should read (bottom to top): 0.5, 0.6, 0.7, 0.8, and 0.9.

In order to calculate the number of particles in the peak, the area must be divided by the width of the defining counter in millivolts. This information was obtained in the following way. Proton-proton scattering peaks were investigated at several angles. At each angle two peaks were taken simultaneously, 1*A*, 2, 3 and 1*B*, 2, 3 against magnet current. These two peaks were, of course, displaced from one another and this displacement was accurately measured. By measuring the distance between the centers of counters 1*A* and 1*B*, the width of counter 1*A* was obtained in millivolts. Dividing by the actual current in the magnet (measured in shunt millivolts), the resolution of the counter was obtained. This is shown in Fig. 6. The decrease in resolving power at high magnetic fields is due to the saturation of the magnet. The resolution can be made independent of magnet current, but high resolving power was not necessary for this experiment.

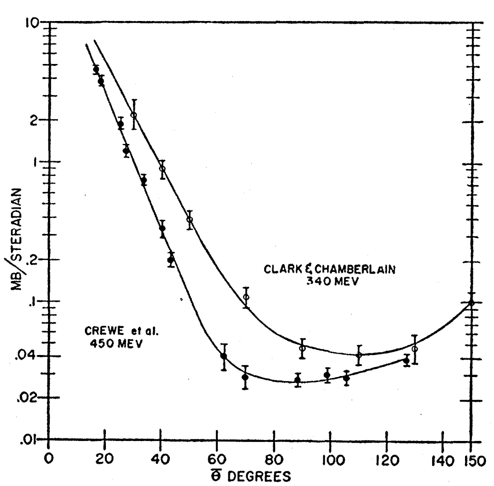

FIG. 7. $(d\sigma_{pd}/d\Omega)(\theta)$ measured in the experiment (black points) compared with results of Chamberlain and Clark for 340-Mev protons on deuterons (circles). (Solid lines are drawn only to guide the eye.)

Table I shows the measured *p*-*d* differential cross sections. The errors which are shown are compounded of statistical errors (both of *p*-*d* and the calibration *p*-*p* measurements), error in normalizing the data from two cyclotron runs, possible errors due to misplacing the center of the peaks, and uncertainties in the resolution. The combined errors due to *p*-*p* calibration and normalization between the two runs is 7.5%. The geometry of the counter telescope was such that losses due to outscattering were negligible. The absorption of deuterons in the target amounted to about 2% and of protons about 0.7%. No correction has been made for this effect.

The measurements were made in two separate cyclotron runs, in only one of which an accurate *p*-*p* calibration was made. Care was taken to measure the *p*-*d* cross section at an identical angle in both runs and this angle was used for inter-calibration. Table I shows the order in which the points were measured in the two cyclotron runs. The differential cross section as a function of the angle in the center-of-mass system is shown in Fig. 7. The results of Chamberlain and Clark at 340 Mev are also shown. Our results show the same general shape and that the cross section continues to fall with increasing incident proton energies.

TABLE I. *p*-*d* differential cross section. The measured cross sections at angles θ or $\bar{\theta}$, the laboratory or c. m. proton scattering angles, respectively. The particle detected is shown. The errors are compounded from the statistical errors, uncertainties in the resolution, normalization with *p*-*p* data, normalization between two cyclotron runs and uncertainties in determining the peak center when protons were detected.[a]

	θ (deg)	$\bar{\theta}$ (deg)	Particle	$d\sigma/d\Omega$ (mb/sterad)	error (%)
XII	10	16.45[b]	*p*	4.64	6.6
IV	11.08	18.2	*p*	3.83	8
II	15.5[c]	25.43	*p*		
XIII	15.5[c]	25.43[b]	*p*	1.90	8
III	16.76	27.43	*p*	1.20	10
I	20.58	33.62	*p*	0.748	9
V	24.88	40.45	*p*	0.336	14
IX	26.68	43.3	*p*	0.201	12
VIII	39.05	62.25	*p*	0.0408	21
X	44.32	69.85	*p*	0.0291	19
XI	44.32	88.4	*d*	0.0277	11
VII	39.05	99.0	*d*	0.0303	12
VI	35.62	105.93	*d*	0.0287	11
XIV	32.9	127.0[b]	*d*	0.0388	8.5

[a] Roman numerals indicate chronological order of data.
[b] Second of two cyclotron runs 3 months apart.
[c] Normalization point between two cyclotron runs.

INTERPRETATION OF THE DATA

Using Eq. (1), we can compute the value of $S(\theta)\Delta$ making use of the values of $d\sigma_{pd}/d\Omega$ measured in this experiment and the values of $d\sigma_{pp}/d\Omega$ and $d\sigma_{np}/d\Omega$ obtained from the literature. We have used the excellent compilation by Hess[7] as our source of information on the latter.

The nucleon-nucleon scattering angle θ' and laboratory bombarding energy T_0' which must be used in this comparison are given by

$$\cos\theta' = \frac{25\cos\theta - 7}{25 - 7\cos\theta}, \tag{3}$$

$$T_0' = \frac{1}{16m} K^2 (25 - 7\cos\theta). \tag{4}$$

K is the center of mass momentum of the proton, m its mass, and θ the center-of-mass angle for the p-d event. These formulas correspond to those of Chamberlain and Clark except that relativistic kinematics have been substituted for classical. Table II gives all the relevant information for calculating $S(\theta)\Delta$. The values are shown plotted against center-of-mass angle in Fig. 8.

The experimental values $S(\theta)\Delta$ were compared with two curves, A and B, showing $S(\theta)$ as computed by the use of Eq. (2). Curve A was obtained by taking the deuteron wave function as

$$\psi_0{}^S(r) = \frac{0.9195}{r}(1 - e^{-2.5r})(1 - e^{-1.59r})(e^{-0.232r} - e^{-1.90r}) \tag{5}$$

$\psi_0{}^S(r)$ was derived by Moravcsik[8] on the basis of Gartenhaus'[9] numerical wave function.

TABLE II. Experimental $S(\theta)\Delta$. The values of $(d\sigma_{np}/d\Omega(\theta')$ and $(d\sigma_{pp}/d\Omega)(\theta')$ used in Eq. (1) are shown. θ' is the nucleon-nucleon scattering angle in c. m. system and T_0' is nucleon-nucleon laboratory bombarding energy corresponding to the p-d energy and $\bar{\theta}$. The relation is shown in Eqs. (3) and (4).

$\bar{\theta}$ (deg)	θ' (deg)	T_0' (Mev)	$\frac{d\sigma_{pp}}{d\Omega}(\theta')$ (mb/sterad)	$\frac{d\sigma_{np}}{d\Omega}(\theta')$ (mb/sterad)	$\left[\frac{9}{16}\frac{\sigma_{pd}}{\sigma_{pp}+\sigma_{np}}\right] = S(\theta)\Delta$
16.45	21.8	465.6	4.4 ±0.4	4.6 ±0.2	0.289 ±0.025
18.2	24.1	467.2	4.2 ±0.4	4.2 ±0.2	0.256 ±0.025
25.43	33.5	475.5	4.1 ±0.3	3.1 ±0.2	0.150 ±0.015
27.43	36.0	478.3	4.0 ±0.3	2.9 ±0.2	0.098 ±0.011
33.62	43.9	488.0	3.90±0.25	2.2 ±0.2	0.069 ±0.007
40.45	52.3	500.9	3.75±0.15	1.7 ±0.2	0.035 ±0.005
43.3	55.8	506.8	3.65±0.10	1.5 ±0.2	0.022 ±0.003
62.25	77.7	553.5	3.30±0.10	0.91±0.1	0.0054±0.0010
69.85	85.9	575.1	3.10±0.10	0.90±0.1	0.0041±0.0008
88.4	104.7	631.5	2.7 ±0.15	1.3 ±0.2	0.0059±0.0006
99.0	114.7	664.3	2.90±0.1	1.8 ±0.2	0.0036±0.0005

[7] W. N. Hess, Revs. Modern Phys. **30**, 368 (1958).
[8] M. J. Moravcsik, Nuclear Phys. **7**, 113 (1958).
[9] S. Gartenhaus, Phys. Rev. **100**, 900 (1955).

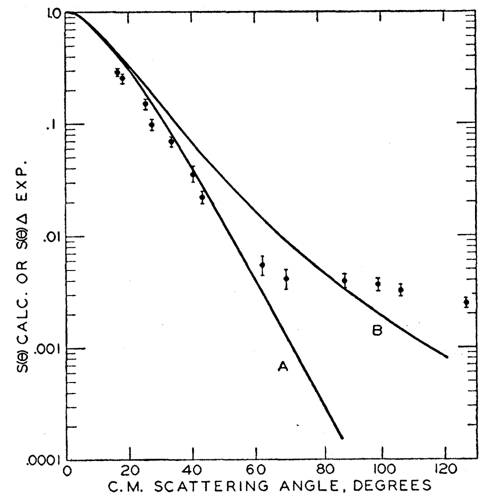

FIG. 8. Sticking factor $S(\theta)$ calculated from Eq. (2): curve A by using an analytical approximation to Gartenhaus' deuteron wave function; curve B by using a Hulthèn wave function. The points are the experimental values of $S(\theta)\Delta$ as listed in Table II.

For higher scattering angles the effect of the D-wave was included by combining 96.86% of $\psi_0{}^S(r)$ with 3.14% of $\psi_0{}^D$ where

$$\psi_0{}^D(r) = \frac{1.0984}{r}(1 - e^{-r})(1 - e^{-2.5r}) \times (0.147e^{-0.256r} + 0.810e^{-0.577r}). \tag{6}$$

The effect of the D-wave was found to be very small. Curve B was obtained from the curve given by Chamberlain and Clark for the Hulthèn potential.

CONCLUSIONS

It can be seen that at small center-of-mass angles the measured points fall below the calculated curve. This may be taken as an indication of destructive interference between p-p and n-p scattering. However, at large angles the measured points are well above the calculated curve. The explanation for this is not clear, but may be due to multiple collisions within the deuteron; that is, events which cannot be correlated directly with elementary nucleon-nucleon collisions at well-defined angles and energies.

ACKNOWLEDGMENTS

We would like to thank Mr. Charles Rey for his assistance in designing some of the apparatus and for his help during the cyclotron runs. We also appreciate the help of Mr. Robert March during the latter part of the experiment.